Thermal Effects in Spin-Torque Switching of Perpendicular Magnetic Tunnel Junctions at Cryogenic Temperatures

L. Rehm,[1,*] G. Wolf,[2] B. Kardasz,[2] E. Cogulu,[1] Y. Chen,[1] M. Pinarbasi,[2] and A.D. Kent[1,†]

[1] *Center for Quantum Phenomena, Department of Physics, New York University, New York, New York 10003, USA*

[2] *Spin Memory Inc., Fremont, California 94538, USA*

(Received 1 September 2020; accepted 1 March 2021; published 30 March 2021)

Temperature plays an important role in spin-torque switching of magnetic tunnel junctions, causing magnetization fluctuations that decrease the switching voltage but also introduce switching errors. Here we present a systematic study of the temperature dependence of the spin-torque-switching probability of state-of-the-art perpendicular-magnetic-tunnel-junction nanopillars (40–60 nm in diameter) from room temperature down to 4 K, sampling up to a million switching events. The junction temperature at the switching voltage—obtained from the thermally assisted spin-torque-switching model—saturates at temperatures below about 75 K, showing that junction heating is significant below this temperature and that spin-torque switching remains highly stochastic down to 4 K. A model of heat flow in a nanopillar junction shows this effect is associated with the reduced thermal conductivity and heat capacity of the metals in the junction.

DOI: 10.1103/PhysRevApplied.15.034088

I. INTRODUCTION

Spintronic devices based on spin-transfer torques [1,2] have attracted a great deal of interest in recent years due to their nonvolatility, energy efficiency, small footprints, fast operation, and high reliability [3–6]. Perpendicularly magnetized magnetic tunnel junctions (pMTJs) are currently the most-promising and most-extensively-studied spin-transfer-torque devices for commercialization because of their high switching efficiency and scaling properties [7,8]. Although the commercial operating temperatures are between −40 and 150 °C, pMTJs have also been recently explored for use as memory elements for a cryogenic computer operating at approximately 4 K [9–11]. Interest in these devices is associated with the need for a high-density low-temperature memory that can be tightly integrated with superconducting logic [12].

It is generally thought that decreasing the device temperature, while increasing the switching voltage, will lead to more-reliable switching. This is because thermal fluctuations introduce randomness in the switching process that produces write errors and read disturbs. These are characterized by a thermal-activation model for spin-torque switching that is also often used to assess key device metrics, including the switching efficiency [13], the ratio of the energy barrier to magnetization reversal to the spin-torque-switching threshold. While studies of devices at and above room temperature are quite common, there are relatively few studies investigating magnetic devices over a broad range of temperatures down to 4 K, the temperature relevant for applications in superconducting electronics. Spin-torque oscillators have been studied at low temperatures [14,15], as has spin-torque switching in all-metallic spin-valve nanopillars [16,17] and the quasistatic response of MgO-based magnetic tunnel junctions [9,18]. High-speed switching (with nanosecond pulses) of magnetic tunnel junctions has also been explored at low temperature [10,11]. However, there have been no studies that we are aware of that explore the switching probability with longer-duration pulses with millions of events at 4 K. The longer pulse durations allow the sample to reach thermal equilibrium and hence analysis of the data with a thermally assisted spin-torque-switching model [19].

In this article, we use the thermally activated spin-transfer-torque-switching model [20–23] to determine the effective switching temperature T_{eff}—the sample temperature at the switching voltage—and the voltage switching threshold from room temperature down to 4 K. Two different methods are used, one based on measurements of the read disturb rate (RDR) and the other on the measurements of the switching voltage versus pulse duration. These are applied to 40- to 60-nm-diameter pMTJs with relatively-low-resistance products ($RA \approx 3\ \Omega\,\mu\mathrm{m}^2$), junctions that exhibit low energy (less than 300 fJ per switch), and fast (subnanosecond) switching at 4 K as reported in Ref. [10]. We find that the switching temperature T_{eff} versus bath temperature saturates below about 75 K. Our findings show

*laura.rehm@nyu.edu

†andy.kent@nyu.edu

that spin-torque switching remains stochastic at cryogenic temperatures.

II. MAGNETIC TUNNEL JUNCTIONS

We investigate magnetic tunnel junctions with a composite $Co_{18}Fe_{54}B_{28}$ (denoted CoFeB) free layer (FL), CoFeB(1.5 nm)/W(0.3 nm)/CoFeB(0.8 nm), and a CoFeB(0.9 nm) reference layer (RL) separated by a 1-nm-thick MgO tunnel barrier. The W layer adds perpendicular magnetic anisotropy and acts as a boron getter during junction annealing. In contrast to room-temperature devices, the FL has only one MgO interface instead of two [24,25], as large perpendicular anisotropy is not needed for low-temperature applications. The RL is coupled to a synthetic antiferromagnet (SAF), which is composed of two Pt/Co multilayers that are antiferromagnetically coupled through a 0.8-nm-thick Ru layer. The layer stack CuN(10 nm)/SAF(9.8 nm)/RL/MgO/FL (see the inset in Fig. 1) is deposited at room temperature and annealed for 25 min at 400 °C. Electron-beam lithography and Ar^+-ion-beam milling are then used to fabricate 40-, 50-, and 60-nm-diameter circular nanopillars.

We first characterize the pMTJ devices by measuring their resistance as a function of applied dc bias voltage at various temperatures between 4 and 295 K. The bias voltage is applied with use of a data-acquisition board (National Instruments PCIe-6353), which simultaneously measures the voltage drop across the tunnel junction and a resistor in series with the junction. The voltage drop across the resistor is used to determine the current flow through the junction. The measurements are performed in a cryogenic probe station where the sample stage can be heated up to 150 K. The room-temperature measurements are performed while the cryostat cold head is turned off.

Figure 1 shows the junction resistance versus bias voltage and voltage-induced switching of a 40-nm pMTJ device at different temperatures in zero applied field. While the resistance in the parallel state R_P (lower-resistance branch in Fig. 1) is almost independent of temperature and bias voltage, the resistance in the antiparallel state R_{AP} (upper branch) shows a strong temperature and bias dependence. This can be attributed to inelastic tunneling processes [26–28]. In the antiparallel state inelastic processes open additional conduction pathways as the bias is increased, leading to this characteristic inverted-V broken-linear response [29]. Figure 1 also shows that the switching voltages $V_{c,AP}$ and $V_{c,P}$ decrease with increasing temperature. The asymmetry of the switching voltages is likely associated with the fringe fields coming from the SAF structure. For this pMTJ we find a bias field of 56 mT at 4 K extracted from field-hysteresis loops that favors the parallel state, lowering $V_{c,AP}$. Our observations are similar to those of earlier studies [9,11]. It is also interesting to note that the pMTJ always switches close to the same resistance values, $R \approx 5849\ \Omega$ for the antiparallel-to-parallel transition and $R \approx 2530\ \Omega$ for the parallel-to-antiparallel transition. The same behavior is observed in 50- and 60-nm-diameter devices.

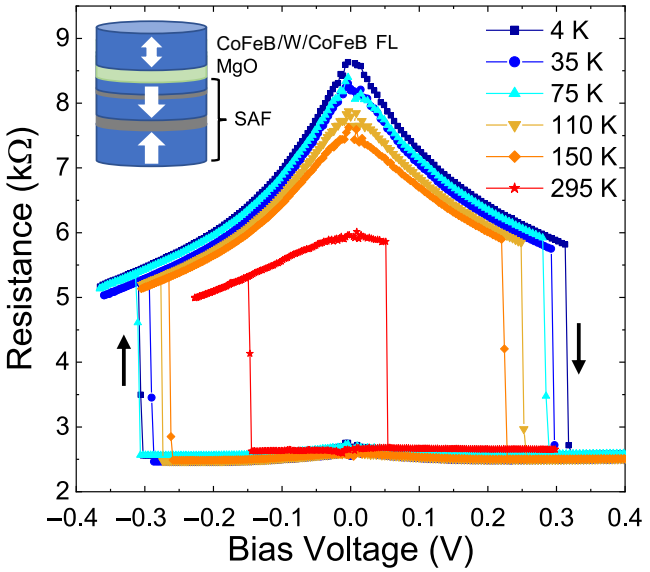

FIG. 1. Quasistatic voltage-induced switching of a 40-nm pMTJ at several temperatures and zero field. The tunneling magnetoresistance ratio around zero applied voltage increases by almost a factor of 2 from 124% at room temperature to 220% at 4 K. The inset shows a schematic of the studied junctions with a CoFeB/W/CoFeB composite free layer.

III. RESULTS AND ANALYSIS

The switching probability is measured and analyzed with the thermally activated spin-transfer-torque-switching model to determine the effective switching temperature and threshold voltages V_{c0} [20–23]. Two methods are used: (i) determination of the switching voltage versus the pulse duration at fixed switching probability and (ii) measurement of the read disturb rate ($P_{sw} \ll 1$) for fixed pulse duration. Both methods have been shown to give reliable estimates of the ratio of the energy barrier to the temperature in magnetic-tunnel-junction devices [19].

In the switching-voltage-versus-pulse-duration method, the device is set in a known state with a reset pulse and then a switching pulse is applied. The state of the pMTJ is measured after the switching pulse, with the junction readout done at a low voltage bias of less than 15 mV, much less than the switching voltage. For each set of pulse conditions, we study 100 events to determine the switching probability as the number of switching events divided by the total number of events. Figure 2(a) shows the switching probability P_{sw} versus the pulse amplitude for pulse durations τ varied over many orders of magnitude, 50 μs to 100 ms. The results shown in Fig. 2(a) are taken at a temperature of 4 K in zero applied field on the same

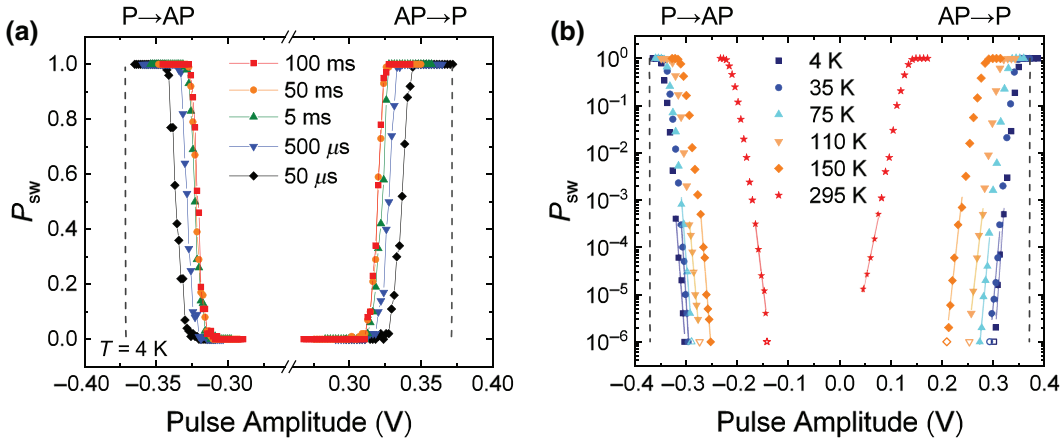

FIG. 2. (a) Switching probability ($P_{\rm sw}$) versus pulsed voltage ramps with various pulse durations of a 40-nm-diameter pMTJ at $T_{\rm bath} = 4$ K and zero field. Each point is an average of 100 switching trials. (b) Switching probability in the low-voltage (read-disturb) limit as a function of voltage-pulse amplitudes for the same device at various temperatures. The pulse duration for this measurement is fixed at 10 μs. The straight lines represent the fits to the data using Eq. (3) described in the main text. The empty data points at 10^6 events stand for no errors and are therefore excluded from the fit. The dashed dark-gray lines in (a),(b) indicate the behavior expected for a device temperature of 4 K. AP refers to the antiparallel magnetization junction state and P to the parallel magnetization state.

40-nm pMTJ as in Fig. 1. See Sec. 1 in Supplemental Material [30] for the experimental results for the 50- and 60-nm devices.

The thermal-activation model relates the switching voltage at fixed switching probability $P_{\rm sw} = 1 - 1/e \simeq 0.63$ to the switching temperature $T_{\rm eff}$ and V_{c0} [19]:

$$V_{\rm sw} = V_{c0}\left[1 - \frac{1}{\Delta}\ln\left(\frac{\tau}{\tau_0}\right)\right], \tag{1}$$

$$\Delta = E_b/k_B T_{\rm eff}, \tag{2}$$

where E_b is the energy barrier to magnetization reversal, τ_0 is the attempt time (approximately 1 ns [16,31]), and Δ is the thermal stability factor, the ratio of the energy barrier to the effective switching temperature. The resulting V_{c0} and Δ values, obtained by our plotting $V_{\rm sw}$ versus the logarithm of the pulse duration, are shown in Figs. 3(a) and 3(b), respectively.

In the RDR method the same experimental procedure is applied but lower-amplitude write pulses are used, pulses for which the switching probability is very small, $P_{\rm sw} \ll 1$. We fix the pulse duration $\tau = 10$ μs and apply up to one million pulses. This again is done as a function of temperature in zero applied field. The resulting probability data are fit to [19]

$$\ln P_{\rm sw} = \ln\left(\frac{\tau}{\tau_0}\right) - \Delta\left(1 - \frac{V}{V_{c0}}\right) \tag{3}$$

to determine V_{c0} and Δ. The fits are shown as straight lines in Fig. 2(b). The hollow data points represent zero errors in 10^6 switching attempts and are excluded from the fits. The resulting values for V_{c0} and Δ obtained by the RDR method can also be found in Figs. 3(a) and 3(b), respectively. V_{c0} and $1/\Delta$ obtained by both methods agree very well [see Figs. 3(a) and 3(b)]. This is expected, as both methods are derived from the same model for thermally activated spin-transfer-torque switching [20–23].

We first discuss and analyze the V_{c0} results. V_{c0} begins to saturate at temperatures less than about 150 K, where $V_{c0,4\ \rm K}$ is 366 and -314 mV and then decreases at room temperature to 215 and -248 mV for the antiparallel-to-parallel transition and the parallel-to-antiparallel transition, respectively [Fig. 3(a)]. We also observe that the temperature dependence is slightly bigger for the antiparallel-to-parallel transition than for the parallel-to-antiparallel transition, which is consistent with the data in Fig. 1. The increased asymmetry of the switching voltages might be related to the fringe field of the reference layer playing a bigger role as the coercive fields of the free layer decrease with increasing temperature [32].

In a macrospin model the intrinsic switching voltage for both switching directions is given by [33]

$$V_{c0} = \alpha\frac{2e}{\hbar}\left(\frac{1+P^2}{P}\right)\frac{\mu_0 M_s H_{k,\rm eff}\mathcal{V}}{G_P} \tag{4}$$

for a symmetric junction, a junction in which the materials on both sides of the tunnel barrier have the same spin polarization. Here α is the damping parameter, e is the elementary charge, $\hbar$ is the reduced Planck's constant, μ_0 is the permeability of free space, M_s is the saturation magnetization, $H_{k,\rm eff}$ is the effective perpendicular anisotropy, $\mathcal{V}$ is the volume of the free layer, G_P is the conductance of the parallel state, and P is the spin polarization, which can be determined from the tunneling magnetoresistance $m_r = 2P^2/(1-P^2)$ [34]. Even in spin-torque switching

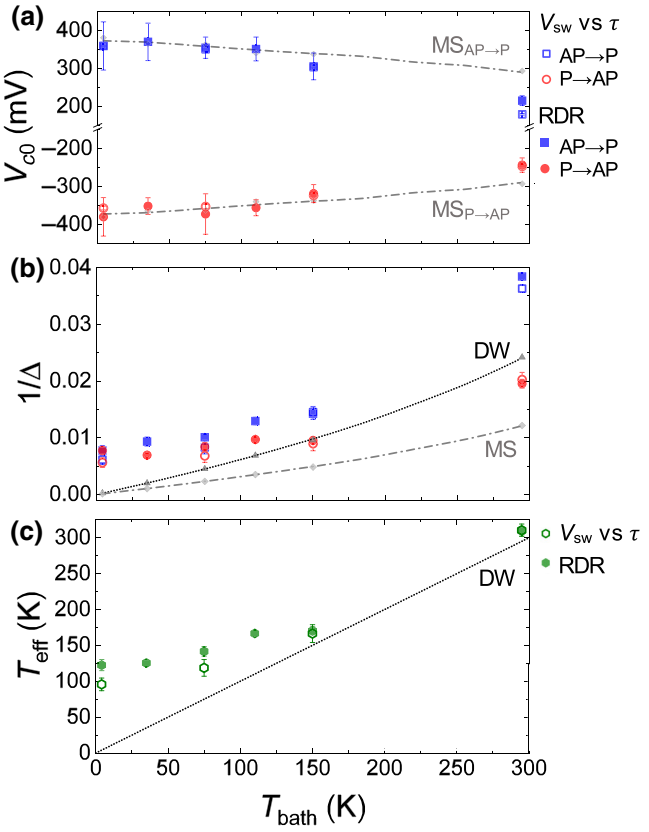

FIG. 3. (a) Intrinsic switching voltage V_{c0}, (b) thermal stability factor Δ, and (c) effective sample temperature T_{eff} from the pulsed voltage ramps and RDR measurements at various temperatures between 4 and 295 K. The dashed gray and dotted black lines represent the expected behavior for the macrospin (MS) model and the domain-wall (DW) model based on material parameters extracted from VSM and FMR measurements, as discussed in the main text. AP refers to the antiparallel magnetization junction state and P to the parallel magnetization state.

that occurs by nucleation and reversed domain expansion, micromagnetic modeling shows that Eq. (4) accurately characterizes the switching threshold [35–37].

To check the correspondence with the expectations of the macrospin model, the variations in free-layer material parameters with temperature are needed. We thus measure the magnetic properties of the layer stacks by vibrating-sample magnetometry (VSM) and ferromagnetic resonance spectroscopy (FMR) in a field-perpendicular geometry in the temperature range from 4 to 295 K. (See Sec. 2 in Supplemental Material [30] for the results.) VSM hysteresis loops of the free layer are used to determine its magnetic moment. The resulting magnetic moment per area unit, $M_s t$, where t is the free layer thickness, for different temperatures can be found in Table I; the values decrease from 1.51 to 1.23 $\times$ 10^{-3} A as the temperature increases, similar to but with a stronger dependence on temperature than results for dual MgO composite free layers [38–40]. Additionally, we also extract the zero-temperature exchange constant A_{ex} for the FL and its dependence on temperature using $A_{\text{ex}}(T) = A_{\text{ex}}(0)(M_s(\text{T}))/(M_s(0))^2$, taking the effective magnetic thickness of this layer to be 1.5 nm [38]. FMR measurements in the field-perpendicular geometry are used to obtain the effective magnetic anisotropy field $H_{k,\text{eff}}$ of the composite FL and account for the demagnetization field associated with its shape [41]. A summary of the results is shown in Table I. We also determine the FL damping parameter α from the FMR linewidth versus frequency to be approximately 0.016 in the whole temperature range. The expectations of the macrospin model for V_{c0} [dashed gray lines in Fig. 3(a)] fit the experimentally obtained data very well for $T_{\text{bath}} \leq 150$ K. The origin of the deviation at 295 K is not entirely clear, but again may be due to the fringe field of the reference layer [32], which is not considered in the macrospin model.

TABLE I. Transport and magnetic properties of the CoFeB/W/CoFeB free layer at selected temperatures. The magnetic properties from FMR and VSM measurements are determined from extended film data as discussed in Sec. 2 in Supplemental Material [30].

T (K)	m_r (%)	$M_s t$ (10^{-3} A)	A_{ex} (pJ/m)	$\mu_0 H_{k,\text{eff}}$ (T)
4	220	1.51	4.2	0.76
35	217	1.49	4.1	0.77
75	211	1.44	3.8	0.76
110	203	1.41	3.7	0.75
150	198	1.37	3.6	0.75
295	124	1.23	2.8	0.67

We now analyze the results shown in Fig. 3(b), which shows the inverse of the thermal stability factor versus bath temperature. As seen from the definition in Eq. (2), $1/\Delta$ is proportional to the temperature and, therefore, if the effective switching temperature were equal to the bath temperature, $1/\Delta$ would have a zero intercept at zero temperature. This is clearly not the case; $1/\Delta$ is nearly independent of temperature below 75 K. We thus conclude that the effective switching temperature is higher than the bath temperature by at least this amount at 4 K.

To be more quantitative we use the FL material parameters and the sample geometry to estimate the energy barrier to reversal as a function of temperature. In the macrospin approximation the energy barrier is given by [13]

$$E_{b,\text{MS}} = K_{\text{eff}} \mathcal{V}, \tag{5}$$

where $K_{\text{eff}} = \mu_0 M_s H_{k,\text{eff}}/2$ is the effective perpendicular anisotropy. Thus, the energy barrier and V_{c0} are dependent on the same temperature-dependent material parameters, notably, M_s and $H_{k,\text{eff}}$. The results in Table I are used to plot the macrospin energy barrier as a function of temperature as the dashed-dotted line in Fig. 3(b).

It is clear that the macrospin model underestimates $1/\Delta$ [Fig. 3(b)] for both switching directions, therefore yielding a clear overestimation of Δ compared with the experimentally obtained values. This is not surprising as the FL is of a size range where we expect the thermally activated reversal to be domain wall mediated. Chavez-O'Flynn *et al.* [41] estimated the critical diameter above which the reversal is by domain-wall motion as $d_c = (16/\pi)\sqrt{A/K_{\rm eff}} \simeq 10$ nm at 4 K, which is much less than the diameter of the FL. In this limit the energy barrier is given by [41]

$$E_{b,\rm DW} = 4\sqrt{A_{\rm ex}K_{\rm eff}}dt, \tag{6}$$

where d is the diameter of the nanopillar. The corresponding $1/\Delta$ values are shown by the dotted black lines in Fig. 3(b) and, as expected, are larger than those of the macrospin model. The domain-wall model thus gives values of $1/\Delta$ that are closer to but still less than the experimental results.

We use the domain-wall model to estimate the effective device switching temperature. First, following common practice, we define Δ as the average value for the antiparallel and parallel states; that is, $\Delta = (\Delta_{\rm AP\to P} + \Delta_{\rm P\to AP})/2$. We find that the domain-wall model describes the data trend at 150 and 295 K well, but still overestimates the values from the measurements below 150 K. Assuming this overestimate is associated with heating, we extract $T_{\rm eff}$ as a function of the cryostat temperature, $T_{\rm bath}$.

The results are shown in Fig. 3(c), with the dotted black line showing $T_{\rm eff} = T_{\rm bath}$. $T_{\rm eff}$ is similar for both the switching-voltage-measurement method and read-disturb-rate-measurement method. Below 150 K, $T_{\rm eff}$ begins to saturate and becomes independent of the bath temperature. At $T_{\rm bath}$ of 4 K, we find a difference between the device temperature and cryostat temperature of $\Delta T_{\rm eff} \approx 118$ K compared with only 14 K at room temperature in the RDR measurements. The same quantities are 92 K at 4 K and 16 K at 295 K in the switching-voltage method versus the pulse-duration method. The current-induced Joule heating we find at room temperature is consistent with the estimate of ΔT of 2–4 K/mW μm^2 from Joule heating $V^2_{\rm applied}/RA$, where RA is the junction's resistance-area product from Refs. [42,43].

While the temperature rise found at room temperature is also consistent with three-dimensional finite-element simulations (COMSOL Multiphysics) of similar magnetic-tunnel-junction stacks with a composite FL at comparable current densities and RA values [44], the saturation of $T_{\rm eff}$ toward lower temperatures cannot be easily explained. To gain further understanding of our experimental findings, we perform COMSOL Multiphysics simulations of 40-nm-diameter pMTJ devices at various bath temperatures down to 4 K. The simulations investigate the steady-state response of the device since the applied microsecond pulses are well beyond the timescales for thermalization. We find that thermal equilibration is reached on the order of nanoseconds, which is also consistent with earlier studies [44,45]. Figure 4(a) shows the temperature distribution at the cross section of our simulated pMTJ device at $T_{\rm bath} = 4$ K. The simulated stack consists of a bottom electrode, three effective tunnel-junction layers, a SAF, an MgO tunnel barrier and FL, a contact plug (capping layer and hard mask), and an adhesion layer with the adjacent top electrode. As expected, the MgO barrier layer is the hottest section of the pillar due to its orders-of-magnitude lower electrical conductivity compared with the other materials in the stack (315 S/m compared with 10^6–10^7 S/m for the metal layers). The average temperature we calculate in the free layer at $T_{\rm bath} = 4$ K is 43 K, which is very close to the maximum temperature in the stack.

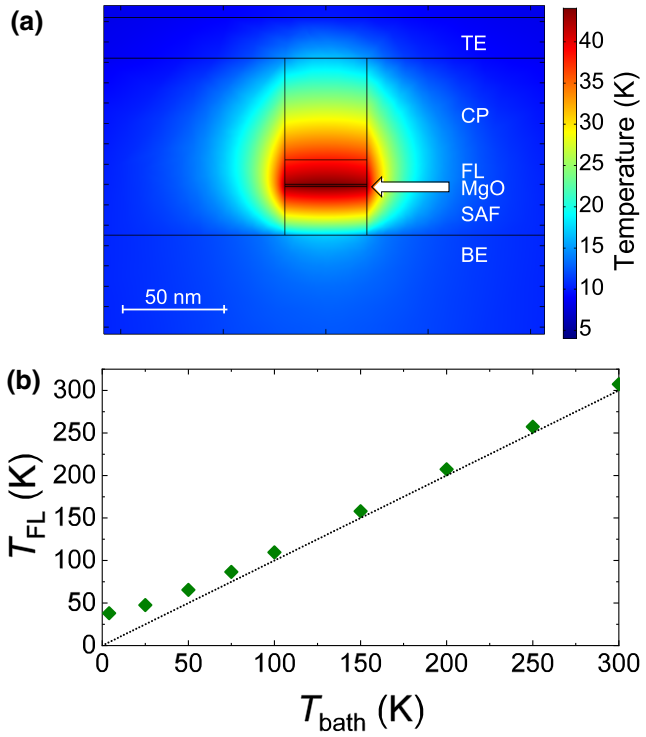

FIG. 4. COMSOL Multiphysics simulation results. (a) Cross-section profile of the thermal map for the simulated 40-nm-diameter pMTJ stack at $T_{\rm bath} = 4$ K stressed with 0.3 V and a device resistance of 2.55 kΩ. (b) Free-layer temperature $T_{\rm FL}$ at various bath temperatures between 4 and 300 K. The dotted black line represents the expected behavior if no heating were to occur. BE, bottom electrode; CP, capping layer and hard mask; TE, top electrode.

Figure 4(b) shows the simulated temperatures in the free layer $T_{\rm FL}$ for bath temperatures up to 300 K. We find that our simulation follows the same behavior we observe in our experimental results [Fig. 3(c)]. At 300 K we find a small temperature rise ΔT of around 9 K and

it stays close to constant down to 100 K. Below 100 K, we observe significant deviations of T_{FL} from the bath temperature [dotted black line in Fig. 4(b)], with ΔT showing the biggest increase at 4 K ($\Delta T = 39$ K). We find that this behavior can be attributed to the fact that the device resistance at the switching point is close to independent of the bath temperature, but the thermal conductivity and heat capacity of our layers decrease with temperature [46,47], especially at temperatures below 100 K. We associate the smaller increase in temperature in our simulations compared with the experiment to the idealizations in our model, such as no thermal contact resistance between the layers and encapsulation layers, and use of material properties associated with magnetic elements instead of alloys. See Sec. 3 in Supplemental Material [30] for a more-detailed description of the simplified stack, the temperature-dependent electrical and thermal conductivity, and the heat capacity of the layers used in our simulation.

IV. CONCLUSION

Our results show that spin-torque switching of pMTJs remains highly probabilistic down to cryogenic temperatures. We associate this with heating of the junction above the bath temperature. Heating becomes more significant as the temperature is reduced as the switching voltage and junction resistance at the switching threshold are nearly independent of temperature but the heat capacity and thermal conductivity of the materials in the junction decrease with decreasing temperature. A further central result of this study is that the switching probability can be described by an effective temperature that becomes independent of the bath temperature at low temperatures. These results are important for furthering our understanding the role of temperature in spin-torque-switching dynamics of pMTJs and their applications as cryogenic memory.

ACKNOWLEDGMENTS

We thank Jamileh Beik Mohammadi for invaluable support and discussions of the VSM measurements. This research was supported in part by Spin Memory Inc.

[1] J. C. Slonczewski, Current-driven excitation of magnetic multilayers, J. Magn. Magn. Mater. **159**, L1 (1996).
[2] L. Berger, Emission of spin waves by a magnetic multilayer traversed by a current, Phys. Rev. B **54**, 9353 (1996).
[3] H. Ohno, T. Endoh, T. Hanyu, N. Kasai, and S. Ikeda, in *2010 International Electron Devices Meeting* (San Francisco, CA, USA, 2010), p. 9.4.1.
[4] J. Park, *et al.*, in *2012 Symposium on VLSI Technology (VLSIT)* (Honolulu, HI, USA, 2012), p. 57.
[5] G. Jan, L. Thomas, S. Le, Y. Lee, H. Liu, J. Zhu, R. Tong, K. Pi, Y. Wang, D. Shen, R. He, J. Haq, J. Teng, V. Lam, K. Huang, T. Zhong, T. Torng, and P. Wang, in *2014 Symposium on VLSI Technology (VLSI-Technology): Digest of Technical Papers* (Honolulu, HI, USA, 2014), p. 1.
[6] S. Ikeda, K. Miura, H. Yamamoto, K. Mizunuma, H. D. Gan, M. Endo, S. Kanai, J. Hayakawa, F. Matsukura, and H. Ohno, A perpendicular-anisotropy CoFeB–MgO magnetic tunnel junction, Nat. Mater. **9**, 721 (2010).
[7] A. D. Kent and D. C. Worledge, A new spin on magnetic memories, Nat. Nanotechnol. **10**, 187 (2015).
[8] B. Jinnai, K. Watanabe, S. Fukami, and H. Ohno, Scaling magnetic tunnel junction down to single-digit nanometers—challenges and prospects, Appl. Phys. Lett. **116**, 160501 (2020).
[9] K. Cao, H. Li, W. Cai, J. Wei, L. Wang, Y. Hu, Q. Jiang, H. Cui, C. Zhao, and W. Zhao, Low-temperature performance of nanoscale perpendicular magnetic tunnel junctions with double MgO-interface free layer, IEEE Trans. Magn. **55**, 1 (2019).
[10] L. Rehm, G. Wolf, B. Kardasz, M. Pinarbasi, and A. D. Kent, Sub-nanosecond spin-torque switching of perpendicular magnetic tunnel junction nanopillars at cryogenic temperatures, Appl. Phys. Lett. **115**, 182404 (2019).
[11] L. Lang, Y. Jiang, F. Lu, C. Wang, Y. Chen, A. D. Kent, and L. Ye, A low temperature functioning CoFeB/MgO-based perpendicular magnetic tunnel junction for cryogenic nonvolatile random access memory, Appl. Phys. Lett. **116**, 022409 (2020).
[12] S. Holmes, A. L. Ripple, and M. A. Manheimer, Energy-efficient superconducting computing-power budgets and requirements, IEEE Trans. Appl. Supercond. **23**, 1701610 (2013).
[13] J. Z. Sun, *et al.* Spin-torque switching efficiency in CoFeB-MgO based tunnel junctions, Phys. Rev. B **88**, 104426 (2013).
[14] J. C. Sankey, I. N. Krivorotov, S. I. Kiselev, P. M. Braganca, N. C. Emley, R. A. Buhrman, and D. C. Ralph, Mechanisms limiting the coherence time of spontaneous magnetic oscillations driven by dc spin-polarized currents, Phys. Rev. B **72**, 224427 (2005).
[15] M. L. Schneider, W. H. Rippard, M. R. Pufall, T. Cecil, T. J. Silva, and S. E. Russek, Temperature dependence of spin-torque-driven self-oscillations, Phys. Rev. B **80**, 144412 (2009).
[16] I. N. Krivorotov, N. C. Emley, A. G. F. Garcia, J. C. Sankey, S. I. Kiselev, D. C. Ralph, and R. A. Buhrman, Temperature Dependence of Spin-Transfer-Induced Switching of Nanomagnets, Phys. Rev. Lett. **93**, 166603 (2004).
[17] G. E. Rowlands, C. A. Ryan, L. Ye, L. Rehm, D. Pinna, A. D. Kent, and T. A. Ohki, A cryogenic spin-torque memory element with precessional magnetization dynamics, Sci. Rep. **9**, 803 (2019).
[18] P. Guo, J. Feng, H. Wei, X. Han, B. Fang, B. Zhang, and Z. Zeng, Temperature dependence of microwave oscillations in magnetic tunnel junctions with a perpendicularly magnetized free layer, Appl. Phys. Lett. **106**, 012402 (2015).
[19] R. Heindl, W. H. Rippard, S. E. Russek, M. R. Pufall, and A. B. Kos, Validity of the thermal activation model for spin-transfer torque switching in magnetic tunnel junctions, J. Appl. Phys. **109**, 073910 (2011).

[20] J. Z. Sun, Spin-current interaction with a monodomain magnetic body: A model study, Phys. Rev. B **62**, 570 (2000).
[21] E. B. Myers, F. J. Albert, J. C. Sankey, E. Bonet, R. A. Buhrman, and D. C. Ralph, Thermally Activated Magnetic Reversal Induced by a Spin-Polarized Current, Phys. Rev. Lett. **89**, 196801 (2002).
[22] R. H. Koch, J. A. Katine, and J. Z. Sun, Time-Resolved Reversal of Spin-Transfer Switching in a Nanomagnet, Phys. Rev. Lett. **92**, 088302 (2004).
[23] Z. Li and S. Zhang, Thermally assisted magnetization reversal in the presence of a spin-transfer torque, Phys. Rev. B **69**, 134416 (2004).
[24] J.-H. Kim, J.-B. Lee, G.-G. An, S.-M. Yang, W.-S. Chung, H.-S. Park, and J.-P. Hong, Ultrathin W space layer-enabled thermal stability enhancement in a perpendicular MgO/CoFeB/W/CoFeB/MgO recording frame, Sci. Rep. **5**, 16903 (2015).
[25] T. Devolder, J. Kim, J. Swerts, S. Couet, S. Rao, W. Kim, S. Mertens, G. Kar, and V. Nikitin, Material developments and domain wall-based nanosecond-scale switching process in perpendicularly magnetized STT-MRAM cells, IEEE Trans. Magn. **54**, 1 (2018).
[26] S. Zhang, P. M. Levy, A. C. Marley, and S. S. P. Parkin, Quenching of Magnetoresistance by Hot Electrons in Magnetic Tunnel Junctions, Phys. Rev. Lett. **79**, 3744 (1997).
[27] C. H. Shang, J. Nowak, R. Jansen, and J. S. Moodera, Temperature dependence of magnetoresistance and surface magnetization in ferromagnetic tunnel junctions, Phys. Rev. B **58**, R2917 (1998).
[28] A. A. Khan, J. Schmalhorst, G. Reiss, G. Eilers, M. Münzenberg, H. Schuhmann, and M. Seibt, Elastic and inelastic conductance in Co-Fe-B/MgO/Co-Fe-B magnetic tunnel junctions, Phys. Rev. B **82**, 064416 (2010).
[29] J. Slonczewski and J. Sun, Theory of voltage-driven current and torque in magnetic tunnel junctions, J. Magn. Magn. Mater. **310**, 169 (2007), Proceedings of the 17th International Conference on Magnetism.
[30] See Supplemental Material at http://link.aps.org/supplemental/10.1103/PhysRevApplied.15.034088 for more details of the switching-voltage-versus-pulse-duration method for all device sizes, the determination of the stack material parameters, and the COMSOL Multiphysics simulation.
[31] W. Wernsdorfer, E. B. Orozco, K. Hasselbach, A. Benoit, B. Barbara, N. Demoncy, A. Loiseau, H. Pascard, and D. Mailly, Experimental Evidence of the Néel-Brown Model of Magnetization Reversal, Phys. Rev. Lett. **78**, 1791 (1997).
[32] M. Lavanant, P. Vallobra, S. Petit Watelot, V. Lomakin, A. D. Kent, J. Sun, and S. Mangin, Asymmetric magnetization switching in perpendicular magnetic tunnel junctions: Role of the synthetic antiferromagnet's fringe field, Phys. Rev. Applied **11**, 034058 (2019).
[33] J. Z. Sun, in *Proc. SPIE 9931* (Spintronics IX, 2016).
[34] M. Julliere, Tunneling between ferromagnetic films, Phys. Lett. A **54**, 225 (1975).
[35] P. Bouquin, S. Rao, G. S. Kar, and T. Devolder, Size dependence of spin-torque switching in perpendicular magnetic tunnel junctions, Appl. Phys. Lett. **113**, 222408 (2018).
[36] J. B. Mohammadi and A. D. Kent, arXiv:2003.13875 [cond-mat.meshall] (2020).
[37] I. Volvach, J. G. Alzate, Y.-J. Chen, A. J. Smith, D. L. Kencke, and V. Lomakin, Thermal stability and magnetization switching in perpendicular magnetic tunnel junctions, Appl. Phys. Lett. **116**, 192408 (2020).
[38] J. B. Mohammadi, B. Kardasz, G. Wolf, Y. Chen, M. Pinarbasi, and A. D. Kent, Reduced exchange interactions in magnetic tunnel junction free layers with insertion layers, ACS Appl. Electron. Mater. **1**, 2025 (2019).
[39] M. Wang, W. Cai, K. Cao, J. Zhou, J. Wrona, S. Peng, H. Yang, J. Wei, W. Kang, Y. Zhang, J. Langer, B. Ocker, A. Fert, and W. Zhao, Current-induced magnetization switching in atom-thick tungsten engineered perpendicular magnetic tunnel junctions with large tunnel magnetoresistance, Nat. Commun. **9**, 671 (2018).
[40] G. Mihajlović, N. Smith, T. Santos, J. Li, M. Tran, M. Carey, B. D. Terris, and J. A. Katine, Origin of the Resistance-Area-Product Dependence of Spin-Transfer-Torque Switching in Perpendicular Magnetic Random-Access Memory Cells, Phys. Rev. Appl. **13**, 024004 (2020).
[41] G. D. Chaves-O'Flynn, G. Wolf, J. Z. Sun, and A. D. Kent, Thermal Stability of Magnetic States in Circular Thin-Film Nanomagnets with Large Perpendicular Magnetic Anisotropy, Phys. Rev. Appl. **4**, 024010 (2015).
[42] R. C. Sousa, I. L. Prejbeanu, D. Stanescu, B. Rodmacq, O. Redon, B. Dieny, J. Wang, and P. P. Freitas, Tunneling hot spots and heating in magnetic tunnel junctions, J. Appl. Phys. **95**, 6783 (2004).
[43] A. Le Goff, V. Nikitin, and T. Devolder, Spin-wave thermal population as temperature probe in magnetic tunnel junctions, J. Appl. Phys. **120**, 023902 (2016).
[44] J. H. NamKoong and S. H. Lim, Temperature increase in nanostructured cells of a magnetic tunnel junction during current-induced magnetization switching, J. Phys. D: Appl. Phys. **42**, 225003 (2009).
[45] D. H. Lee and S. H. Lim, Increase of temperature due to Joule heating during current-induced magnetization switching of an MgO-based magnetic tunnel junction, Appl. Phys. Lett. **92**, 233502 (2008).
[46] A. L. Woodcraft, Predicting the thermal conductivity of aluminium alloys in the cryogenic to room temperature range, Cryogenics **45**, 421 (2005).
[47] T. Ying, H. Chi, M. Zheng, Z. Li, and C. Uher, Low-temperature electrical resistivity and thermal conductivity of binary magnesium alloys, Acta Mater. **80**, 288 (2014).